# Quantitative scales for haliphilicity of metals: Tailoring the halide affinity of alkaline earth metals to synthesize chalcogenide perovskite $BaMS_3$ (M= Zr, and Hf) and $Cu_2BaSnS_4$ compounds

Shubhanshu Agarwal[a], Kiruba Catherine Vincent[a], and Rakesh Agrawal[*,a]

[a]Davidson School of Chemical Engineering, Purdue University, West Lafayette, IN 47907(USA)

*Corresponding author: Dr. Rakesh Agrawal. E-mail: agrawalr@purdue.edu

**Keywords:** Metal Chlorides, Chloriphilicity Scale, Chalcogenide Perovskites, Solution-Processing, Low-Temperature, $BaZrS_3$, $Cu_2BaSnS_4$

**Abstract**

Chalcogenide semiconductors, such as $BaMS_3$ (M=Zr and Hf) and $Cu_2BaSnS_4$, have attracted growing interest due to the constituent elements' abundance and reported promising properties. However, the synthesis of these alkaline earth-containing chalcogenides from commonly available metal halides has generally been unsuccessful and has traditionally relied on expensive organometallic precursors or vacuum processing techniques, which hinder widespread research on these materials. In this study, we conducted thermodynamic calculations and developed chloriphilicity and iodiphilicity scales for various metals, leveraging their relative affinities for chlorine and iodine respectively, compared to their corresponding metal sulfides. Utilizing these scales, we introduced a $K_2S$-$H_2S$ system to address the affinity of alkaline earth metals for chlorine and iodine. This approach enables the synthesis of these intriguing chalcogenide materials through solution-based methods using metal chloride and metal iodide precursors. This system demonstrates remarkable efficacy for both sulfide and selenide semiconductors.

## 1. Introduction

Chalcogenide materials have been extensively investigated for various optoelectronic applications, including LEDs, photovoltaics, sensors, and more.[1–3] These materials typically exhibit robust stability in the presence of air and moisture, along with diverse optical bandgaps and intriguing properties.[4–7] Examples such as $Cu(In,Ga)(S,Se)_2$, $Cu_2ZnSn(S,Se)_4$, and $Sb_2Se_3$ are actively explored for photovoltaic purposes.[7–9] Thin absorber films of these materials have been deposited using various methods, ranging from co-sputtering to nanocrystal inks and molecular precursor deposition techniques. [10–13] Among these, molecular precursor approaches have emerged as a cost-effective roll-to-roll deposition method, yielding the highest efficiencies among solution-deposited methods.[14,15]

The metal precursors used in such syntheses can include metal-organic compounds, organometallics, metal salts (such as metal halides and metal acetylacetonates), metal chalcogenides, and pure metals.[16–18] While pure metals and metal chalcogenides could be attractive for synthesizing impurity-free chalcogenides, the chemistries required to dissolve such precursors often involve highly toxic and flammable solvents.[19,20] The high cost of oxygen-free metal-organic and organometallic precursors can negate the cost benefits of

solution-processing routes. Therefore, metal salt precursors are a viable option for the cost-effective and easily scalable production of solution-processed chalcogenide films. Among these, metal chlorides have been increasingly used in dimethyl formamide-thiourea complexation chemistry to synthesize highly efficient $Cu(In,Ga)(S,Se)_2$ and $Cu_2ZnSn(S,Se)_4$ solar cells.[21,22]

In addition to well-established chalcogenide materials, emerging chalcogenides such as chalcogenide perovskites and kesterite-inspired $Cu_2BaSnS_4$ show great promise for various optoelectronic applications.[23–27] Chalcogenide perovskites, which are comparable to halide perovskites in their structure and potentially in optoelectronic properties, hold significant promise for tandem solar cells.[25,28–30] Similarly, $Cu_2BaSn(S,Se)_4$ is proposed as a promising alternative to $Cu_2ZnSn(S,Se)_4$, suitable for both single-junction and tandem solar cells.[31] However, despite their potential, chalcogenide perovskites have faced challenges due to the high synthesis temperatures, often exceeding 1000°C.[30,32–34] Recent advancements, including our group's work, have successfully lowered the synthesis temperature of $BaMS_3$ (M=Zr, Hf) chalcogenide perovskites to below 600°C using a $BaS_x$ liquid flux.[35,36] This approach has enabled novel solution-processing routes, though many still rely on costly organometallic precursors.[37–40] In the long term, synthesizing these compounds with cost-effective precursors is crucial for reducing manufacturing costs. While metal salt precursors such as metal chlorides have been successfully used for compounds like $Cu(In,Ga)(S,Se)_2$ and $Cu_2ZnSn(S,Se)_4$, their implementation in the solution-processed synthesis of $BaMS_3$ compounds is hindered by the high affinity of alkaline earth metals for halides.[41] Similarly, solution-processed $Cu_2BaSnS_4$ reports are limited and often contain sulfate impurities or use non-benign solvents.[42] Our study addresses these challenges by employing thermodynamic calculations to determine the affinities of metals to chlorine and iodine relative to sulfides, optimizing the sulfurization step to utilize metal halide precursors for synthesizing $BaMS_3$ and $Cu_2BaSnS_4$ compounds. Carbon has been identified as a problematic impurity in solution-processed chalcogenide films due to its adverse effects on grain growth and composition. In this study, we present the first report on the fabrication of carbon-free thin films of $BaZrS_3$ from chloride precursors.

## 2. Experimental Details

### *2.1. Materials and Characterization*

Barium chloride ($BaCl_2$, 99.5%), zirconium (IV) chloride (ZrCl4, 99.5%), barium iodide ($BaI_2$, anhydrobeads, 99.995%), hafnium (IV) chloride ($HfCl_4$, 99.9%), copper (I) chloride (CuCl, 99.995%), tin (II) chloride ($SnCl_2$, anhydrous, 99.99%), indium chloride ($InCl_3$, 99.999%), calcium chloride ($CaCl_2$, 97%), N,N-dimethylformamide (anhydrous, 99.8%), sulfur flakes (99.99%), selenium powder (99.99%), and alumina dispersed in isopropanol (20 wt%) were purchased from Sigma-Aldrich. Zirconium (IV) iodide ($ZrI_4$, 99.5%) and potassium sulfide ($K_2S$, 95%) were procured from Strem Chemicals. Titanium (IV) chloride ($TiCl_4$, 99.99%), strontium iodide ($SrI_2$, 99.99%), strontium chloride ($SrCl_2$, 99.5%), and thiourea (99%) were obtained from Fisher Scientific. Hafnium hydride ($HfH_2$, 99.9%) was purchased from Nano Research Elements. Borosilicate glass ampules were sourced from Chemglass, and quartz microscope slides were acquired from Quartz Scientific.

All chemicals were stored in nitrogen-filled gloveboxes. Metal precursors and dimethylformamide were used as received. Thiourea was recrystallized twice using DI water, following the procedure detailed elsewhere. Sulfur flakes were ground into a fine powder using a mortar and pestle inside the glovebox, then

dried under vacuum on a Schlenk line at 60°C for 24 hours. Similarly, selenium powder was dried under vacuum at 100°C for 24 hours.

A thin alumina layer was coated on the quartz slides to enhance the spreading of ink during coating and prevent metal diffusion into the quartz. Before alumina deposition, quartz slides were thoroughly rinsed with DI water, organic solvents such as isopropanol and methanol, and a soap solution to remove surface contaminants. The slides were then rinsed again with DI water and treated in a UV-ozone cleaner for 30 minutes. A commercial alumina solution was diluted by mixing 0.2 ml of the solution with 1.8 ml of isopropanol. The diluted solution was spin-coated onto the cleaned quartz slide at 1000 RPM for 1 minute, followed by annealing at 100°C for 1 minute and then at 500°C for 30 minutes.

It is important to note that $TiCl_4$ reacts vigorously with water and should be handled in a moisture-free environment. In this study, it was handled in a nitrogen-filled glovebox.

It should be noted that the purity of $K_2S$ is a concern, as we occasionally observed sodium impurities in our samples, likely originating from impure $K_2S$. Sodium volatiles might have interacted with the film during synthesis. The $K_2S$ we obtained from Strem Chemicals was marketed as 95% pure. Furthermore, based on our calculations, $Na_2S$-$H_2S$ should also be capable of shuttling chlorine from the Ba-Zr-S-Cl film to sodium. However, we observed significant impurities of $Na_2ZrS_3$ in the film, possibly due to the volatility of Na-S compounds in the presence of excess sulfur in the ampule. Therefore, modifications to the heat treatment process are necessary if $Na_2S$ is to be used as a halide sink.

X-ray diffraction analysis was conducted using a Rigaku SmartLab Diffractometer under ambient conditions, employing parallel beam geometry with an incident beam angle of 0.5 degrees. Data collection utilized a Cu Kα source (λ = 1.5406 Å) operated at 40 kV and 44 mA.

Scanning electron microscopy (SEM) and Energy Dispersive X-ray measurements (EDX) were performed using the FEI Nova three-dimensional system equipped with an Everhart Thornley detector. The measurements were carried out at an accelerating voltage of 10 kV with a working distance of 5 mm.

Raman spectroscopy was performed using a Horiba/Jobin-Yvon HR800 Raman spectrometer with a 632.8 nm excitation laser wavelength with approximately 0.05 μW laser power in backscattering configuration at room temperature. The spectra were calibrated based on silicon reference Raman spectrum.

Reflectance data were obtained using a PerkinElmer Lambda 950 spectrometer equipped with an integrating sphere. The data were collected with a 3 mm x 2 mm spot size and a collection time of 1 nm/sec, and were analyzed using the Tauc equation for direct bandgap estimation. We analyzed the Tauc plots following the best practices established in the literature.[66,67]

### *2.2. Synthesis methods*

#### *2.2.1. Ink Preparations*

<u>$AS_x$ (A=Ba, Sr, Ca and x=1,2,3) synthesis from metal chlorides</u>

We initially weighed $BaCl_2$ and thiourea into a vial with target molarities of 0.2 M and 4 M, respectively, inside a nitrogen-filled glovebox. This was followed by the addition of dimethyl formamide in the glovebox to achieve the desired molarities of the precursors. The solution was stirred at 35 °C overnight to completely dissolve the precursors in the solvent. A similar procedure was followed for preparing $SrCl_2$ and $CaCl_2$ solutions in dimethyl formamide with thiourea.

The resulting solutions were doctor blade coated onto 1" x 1" alumina-coated quartz slides. For each layer, 50 µL of ink was used, with the blade moving at a speed of 15 mm per sec. The as-coated film was then annealed on a hotplate at 350 °C. A total of 8 layers were applied. The resulting film was then divided into four 1" x 0.25" pieces inside the glovebox, and one piece was sulfurized in a borosilicate ampule in the presence of $HfH_2$, $K_2S$, and sulfur.

$BaMS_3$ (M=Hf, Zr, Ti) synthesis from metal chlorides

We initially weighed $BaCl_2$, $ZrCl_4$ and thiourea into a vial with target molarities of 0.2 M, 0.2 M and 6 M, respectively, inside a nitrogen-filled glovebox. This was followed by the addition of dimethyl formamide in the glovebox to achieve the desired molarities of the precursors. The solution was stirred at 35 °C overnight to completely dissolve the precursors in the solvent. A similar procedure was followed to prepare other solutions, replacing $ZrCl_4$ with $TiCl_4$ and $HfCl_4$, respectively.

The resulting solutions were doctor blade coated onto 1" x 1" alumina-coated quartz slides. For each layer, 50 µl of ink was used, with the blade moving at a speed of 15 mm per sec. The as-coated film was then annealed on a hotplate at 350 °C. A total of 12 layers were applied. The resulting film was then divided into four 1" x 0.25" pieces inside the glovebox, and one piece was sulfurized in a borosilicate ampule in the presence of $HfH_2$, $K_2S$, and sulfur.

$Cu_2BaSnS_4$ synthesis from metal chlorides

We initially weighed CuCl, $BaCl_2$, $SnCl_2$ and thiourea into a vial with target molarities of 0.2 M, 0.1 M, 0.1 M and 6 M, respectively, inside a nitrogen-filled glovebox. This was followed by the addition of dimethyl formamide in the glovebox to achieve the desired molarities of the precursors. The solution was stirred at 35 °C overnight to completely dissolve the precursors in the solvent.

The resulting solution was doctor blade coated onto 1" x 1" alumina-coated quartz slides. For each layer, 50 µl of ink was used, with the blade moving at a speed of 15 mm per sec. The as-coated film was then annealed on a hotplate at 350 °C. A total of 12 layers were applied. The resulting film was then divided into four 1" x 0.25" pieces inside the glovebox, and one piece was sulfurized in a borosilicate ampule in the presence of $HfH_2$, $K_2S$, and sulfur.

$AS_x$ (A=Ba, Sr, Ca and x=1,2,3) synthesis from metal iodides

We initially weighed $BaI_2$ and thiourea into a vial with target molarities of 0.2 M and 4 M, respectively, inside a nitrogen-filled glovebox. This was followed by the addition of dimethyl formamide in the glovebox to achieve the desired molarities of the precursors. The solution was stirred at 35 °C overnight to completely

dissolve the precursors in the solvent. A similar procedure was followed for preparing $SrI_2$ solution in dimethyl formamide with thiourea.

The resulting solutions were doctor blade coated onto 1" x 1" alumina-coated quartz slides. For each layer, 50 µl of ink was used, with the blade moving at a speed of 15 mm per sec. The as-coated film was then annealed on a hotplate at 350 °C. A total of 8 layers were applied. The resulting film was then broken into four 1" x 0.25" pieces inside the glovebox, and one piece was sulfurized in a borosilicate ampule in the presence of $HfH_2$, $K_2S$, and sulfur.

$BaZrS_3$ synthesis from metal iodides

We initially weighed $BaI_2$, $ZrI_4$ and thiourea into a vial with target molarities of 0.2 M, 0.2 M and 6 M, respectively, inside a nitrogen-filled glovebox. This was followed by the addition of dimethyl formamide in the glovebox to achieve the desired molarities of the precursors. The solution was stirred at 35 °C overnight to completely dissolve the precursors in the solvent.

The resulting solutions were doctor blade coated onto 1" x 1" alumina-coated quartz slides. For each layer, 50 µl of ink was used, with the blade moving at a speed of 15 mm per sec. The as-coated film was then annealed on a hotplate at 350 °C. A total of 12 layers were applied. The resulting film was then broken into four 1" x 0.25" pieces inside the glovebox, and one piece was sulfurized at a time in a borosilicate ampule in the presence of $HfH_2$, $K_2S$, and sulfur.

$BaIn_2S_4$ synthesis from metal chlorides

We initially weighed $BaCl_2$, $InCl_3$ and thiourea into a vial with target molarities of 0.1 M, 0.2 M and 6 M, respectively, inside a nitrogen-filled glovebox. This was followed by the addition of dimethyl formamide in the glovebox to achieve the desired molarities of the precursors. The solution was stirred at 35 °C overnight to completely dissolve the precursors in the solvent.

The resulting solution was doctor blade coated onto 1" x 1" alumina-coated quartz slides. For each layer, 50 µl of ink was used, with the blade moving at a speed of 15 mm per sec. The as-coated film was then annealed on a hotplate at 350 °C. A total of 12 layers were applied. The resulting film was broken into four 1" x 0.25" pieces inside the glovebox, and one piece was sulfurized in a borosilicate ampule in the presence of $HfH_2$, $K_2S$, and sulfur.

### *2.2.2. Ampule heat treatment*

The coated and hot plate-annealed film was transferred to a 5 ml borosilicate glass ampule inside the glovebox, along with 11 mg of sulfur, 5 mg of $HfH_2$, and 0.2 mg of $K_2S$ (15 mg of selenium instead of sulfur in the case of $BaSe_3$). The $HfH_2$ and sulfur were packed together in a thin borosilicate tube with an outer diameter of 3 mm, and the tube was plugged with quartz wool to prevent the escape of $HfH_2$ powder and contamination of the film. Similarly, $K_2S$ powder was packed in a separate 3 mm borosilicate tube, also plugged with quartz wool. Subsequently, the glass ampule was connected to a vacuum rubber tubing, and the other end was attached to a Teflon vacuum valve. This setup was taken out of the glovebox and

connected to a Schlenk line, where the headspace above the Teflon valve was purged multiple times using vacuum-argon cycles. The valve was then opened, and the glass ampule was purged three times with vacuum-argon cycles before sealing the ampule with a butane-air portable hand torch at pressures below 200 mtorr.

## 3. Results and Discussion

### *3.1. Thermodynamic Calculations*

The affinity for chlorine varies across the periodic table, yet comprehensive calculations on this aspect have not been presented in any existing report. While there are studies regarding the high chlorine affinity of alkaline earth metals, their affinity relative to other metals remains unclear.[43,44] This study assessed the room-temperature standard enthalpy of formation and entropy for various metal sulfides and metal chlorides sourced from multiple references and calculated the standard Gibbs free energy of formation, see **Tables S1 and S2**.[45–47] Subsequently, we calculated the difference in the Gibbs free energy of formation between metal chloride and metal sulfide using the following methodology (data available in the Supporting Information (SI) **Table S3**):

$\Delta_f G^0_o = \Delta_f G^0_s(M_2S_{2n+1}) - 2*\Delta_f G^0_c(MCl_{2n+1})$ (if oxidation state of metal is 2n+1 where n=0,1,2,3…..)
$\Delta_f G^0_o = \Delta_f G^0_s(MS_n) - \Delta_f G^0_c(MCl_{2n})$ (if oxidation state of metal is 2n where n=1,2,3…..)

Here, $\Delta_f G^0_o$ refers to the difference in the Gibbs free energy of formation between metal sulfide and metal chloride, $\Delta_f G^0_s$ refers to the standard Gibbs free energy of formation of metal sulfide, $\Delta_f G^0_c$ refers to the standard Gibbs free energy of formation of metal chloride, and M denotes the metal. The difference was then normalized by the theoretical number of metal-chlorine bonds formed in one formula unit of the metal chloride (see **Table S3**), as follows:

No. of bonds: 2(2n+1) (if oxidation state of metal is 2n+1 where n=0,1,2,3…..)
No. of bonds: 2n (if oxidation state of metal is 2n where n=1,2,3…..)

The higher the difference, the more difficult it is to convert metal chloride to metal sulfide by sulfurization. This normalized Gibbs free energy difference was referred to as $\Delta_f G^0_n$ in the supporting information. We further normalized the difference with respect to the metal with the highest value according to the following scheme:

$$\text{Chloriphilicity} = (\Delta_f G^0_{n,i} - \Delta_f G^0_{n,min})/(\Delta_f G^0_{n,max} - \Delta_f G^0_{n,min})$$

This provides a chloriphilicity scale for metals, ranging from 0 to 1, where 1 represents the highest chloriphilicity and 0 is the lowest, as shown in **Table 1**. These calculations distinctly reveal that alkaline earth metals rank among the most chloriphilic elements in the periodic table. However, on average, alkali metals appear to exhibit much greater chloriphilicity than alkaline earth metals. For instance, according to the chloriphilicity scale, Na and K demonstrate higher chloriphilicity than all alkaline earth metals. This suggests that the following reaction should be thermodynamically favorable:

$MX_2 + N_2S \rightarrow MS + 2NX$ where M = Sr, Ca, Ba and N = Na, K

However, the preceding calculations were conducted at room temperature. Therefore, we conducted temperature-dependent thermodynamic calculations for the subsequent reaction:

$BaCl_2+K_2S \rightarrow 2KCl+BaS$

The temperature-dependent $\Delta_f H^0(T)$ and $S^0(T)$ values for the compounds were obtained from the NIST webbook and supplemented with other sources wherever required. The methodology to calculate $\Delta_f G^0(T)$ is outlined in the SI. The calculations indicate that the reaction is thermodynamically favorable at all temperatures including 900°C (depicted in **Figure 1.a**). This suggests that disregarding kinetic barriers, the reaction should be capable of synthesizing barium sulfide from barium chloride using potassium sulfide. However, a significant hurdle is the kinetic barrier due to diffusion limitations. The reaction kinetics are expected to be sluggish as both reactants are in solid form.

The kinetic diffusion challenge can be circumvented by employing a shuttle gas capable of transferring chlorine between $BaCl_2$ and $K_2S$. One potential option is $H_2S$. Despite its small introduction, $H_2S$ can react with $BaCl_2$ to produce BaS and HCl in equilibrium, as depicted in **Figure 1.b** showcasing the temperature-dependent equilibrium constant ($K_{eq}$). Notably, calculations for KCl in **Figure 1.b** indicate a significantly smaller $K_{eq}$ compared to $BaCl_2$, suggesting that *Reaction 1* would be more thermodynamically favorable than *Reaction 2*. Consequently, introducing $H_2S$ should facilitate chlorine transfer from barium to potassium. In summary, the reaction involving $BaCl_2$, $H_2S$, and $K_2S$ offers a mechanism to shuttle chlorine between barium and potassium.

$BaCl_2+H_2S \rightarrow BaS+2HCl$, …… (1)

$2KCl+H_2S \rightarrow K_2S+2HCl$, …… (2)

The schematic in **Figure 2** summarizes the proposed reaction mechanism. Similar calculations have been performed to assess the iodine affinity of different elements, and the scale is available in the supporting information (see **Tables S4-S7**). The trend persists, wherein alkali metals exhibit a greater affinity to iodine compared to alkaline earth metals. Additional calculations indicate that $H_2S$ should likewise facilitate the transfer of iodine between barium and potassium (depicted in **Figure S1**).

**Table 1:** List of the chloriphilicity of common elements calculated using the normalized Gibbs free energy differences between the metal sulfide and metal chloride. The element with the highest free energy difference was assigned a value of 1. The more chloriphilic elements preferentially form bonds with chlorine rather than sulfur.

| Element | Oxidation State | Chloriphilicity scale |
|---|---|---|
| Pt | +2 | 0.00 |
| Ir | +3 | 0.11 |
| C | +4 | 0.11 |
| Mo | +4 | 0.16 |
| Rh | +3 | 0.23 |
| Cu | +2 | 0.26 |
| Sn | +4 | 0.26 |

| Element | Oxidation State | Chloriphilicity scale |
|---|---|---|
| Ag | +1 | 0.39 |
| B | +3 | 0.39 |
| Ni | +2 | 0.39 |
| Al | +3 | 0.40 |
| Dy | +3 | 0.40 |
| Tb | +3 | 0.40 |
| Ho | +3 | 0.40 |

| | | | | | |
|---|---|---|---|---|---|
| As | +3 | 0.28 | Cd | +2 | 0.41 |
| U | +4 | 0.29 | Gd | +3 | 0.42 |
| Hf | +4 | 0.31 | Fe | +2 | 0.44 |
| Zr | +4 | 0.31 | Co | +2 | 0.44 |
| Hg | +2 | 0.31 | Th | +4 | 0.45 |
| Ga | +3 | 0.31 | Sm | +3 | 0.45 |
| Ti | +4 | 0.31 | Cr | +3 | 0.46 |
| Ge | +4 | 0.31 | Pb | +2 | 0.46 |
| Lu | +3 | 0.32 | Be | +2 | 0.47 |
| In | +3 | 0.33 | Mn | +2 | 0.47 |
| Sn | +2 | 0.33 | Nd | +3 | 0.50 |
| Sb | +3 | 0.34 | La | +3 | 0.50 |
| Cu | +1 | 0.35 | Pr | +3 | 0.52 |
| Si | +4 | 0.35 | Mg | +2 | 0.53 |
| Sc | +3 | 0.35 | Ca | +2 | 0.57 |
| H | +1 | 0.35 | Tl | +1 | 0.57 |
| Bi | +3 | 0.36 | Sr | +2 | 0.64 |
| Tm | +3 | 0.37 | Li | +1 | 0.68 |
| Zn | +2 (beta phase) | 0.37 | Ba | +2 | 0.72 |
| V | +3 | 0.37 | Na | +1 | 0.84 |
| Y | +3 | 0.39 | K | +1 | 0.91 |
| Er | +3 | 0.39 | Rb | +1 | 0.96 |
| Zn | +2 (alpha phase) | 0.39 | Cs | +1 | 1.00 |

*3.2. Synthesis of alkaline earth sulfides from chloride precursors*

This section discusses the innovative approach of shuttling chlorine between barium and potassium, as discussed earlier, to synthesize alkaline earth metal sulfides. The chemistry involving thiourea complexation in dimethyl formamide (DMF) has demonstrated the ability to dissolve various metal chlorides and is recognized for generating carbon-free chalcogenide films.[21] Therefore, we have investigated this chemistry for dissolving alkaline earth chlorides, with detailed dissolution procedures outlined in the experimental section.

The $BaCl_2$-thiourea-DMF solution was blade-coated and annealed on a hot plate at 350°C, followed by sulfurization in an ampule containing sulfur, $HfH_2$, and $K_2S$. X-ray fluorescence (XRF) measurements of the as-annealed film confirmed the presence of chlorine (depicted in **Figures S2 and S3**). During sulfurization, sulfur reacted with $HfH_2$ to form $HfS_3$, releasing $H_2S$ gas. This $HfS_3$-$H_2S$ shuttle system aided in removing any remaining oxygen from the film, as outlined in our recent group report.[48] Additionally, it

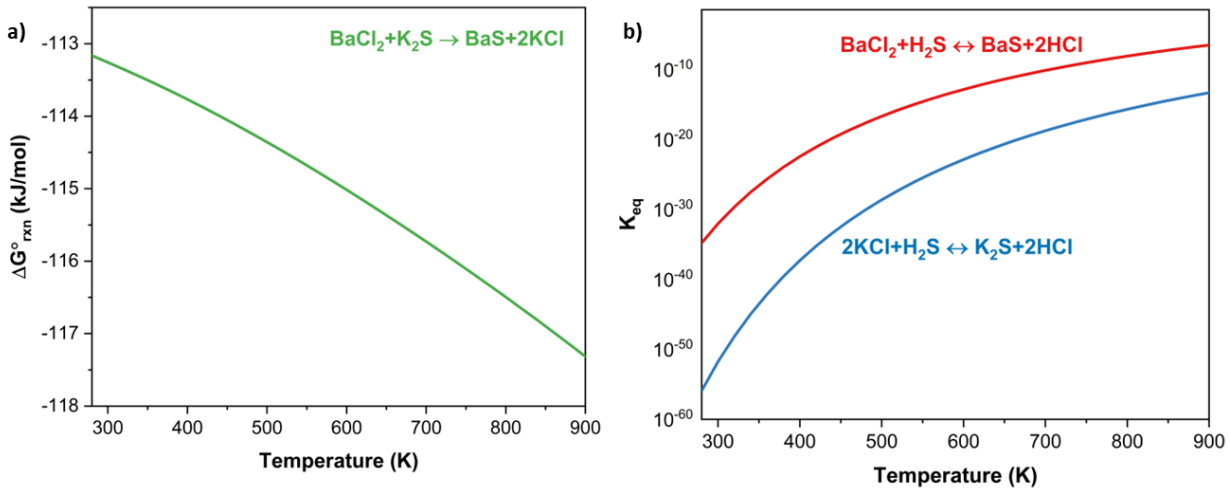


**Figure 1:** a) Temperature-dependent Gibbs free energy of reaction, b) Equilibrium constant as a function of temperature for the reactions at the $BaCl_2$ sample and $K_2S$ chlorine sink with the $H_2S$/HCl shuttle.

is hypothesized that the $K_2S$-$H_2S$ system facilitated the removal of chlorine from the barium film, transferring it to potassium. The film was sulfurized at 500°C for 36 hours, resulting in phase-pure $BaS_3$, as confirmed by X-ray diffraction (illustrated in **Figure 3.a**). We observed significant grain orientation in the film, resulting in a highly oriented $BaS_3$ structure, consistent with previous literature reports.[35] Despite this orientation, we successfully indexed the X-ray diffraction pattern, confirming the presence of all major peaks (see **Figure S4**). The Raman spectrum of the sample also matches the standard reported in the literature (see **Figure S5**). Furthermore, Energy Dispersive X-ray (EDX) analysis of the $BaS_3$ sample revealed a nearly 1:3 Ba to S ratio, further validating our findings, as shown in **Figure S6**. The successful transfer of chlorine from the film to the $K_2S$ was confirmed by XRF measurement shown in **Figure S7**, which detected the presence of K, Cl, and S in the original $K_2S$ powder after sulfurization, supporting our hypothesis. A similar synthesis attempt without the use of $K_2S$ resulted in residual $BaCl_2$ in the film, as shown in **Figure S8**.

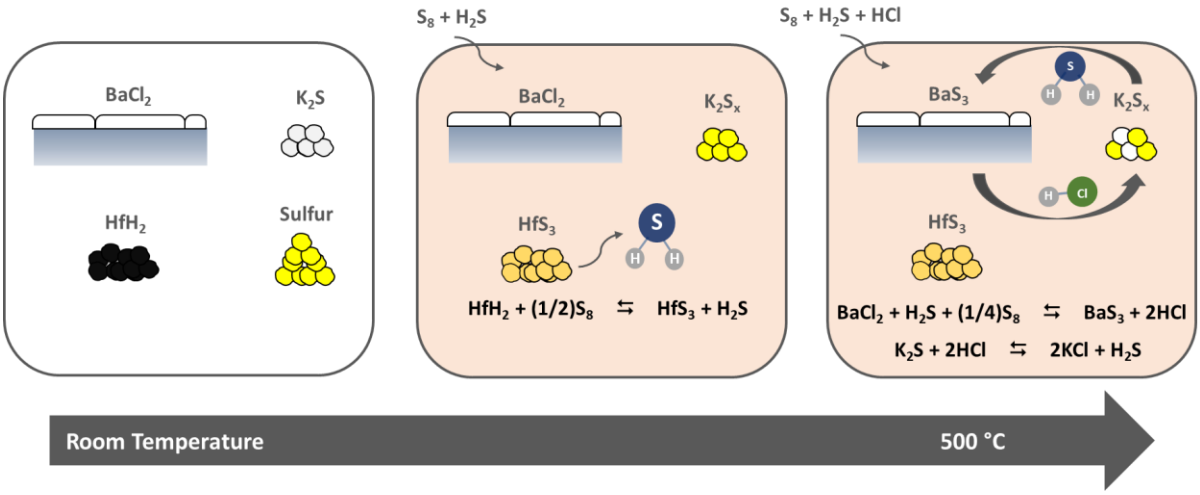


**Figure 2:** Schematic of the proposed sulfurization method to convert $BaCl_2$ into $BaS_3$. This method generates in-situ $H_2S$ and HCl, which shuttles chlorine from Ba to highly chloriphilic K.

Similarly, films based on $CaCl_2$-thiourea-DMF and $SrCl_2$-thiourea-DMF were sulfurized using sulfur-$HfH_2$-$K_2S$ at 500°C, resulting in phase-pure CaS and SrS (shown in **Figures 3.b and 3.c**). Moreover, this approach can be readily extended to selenides, as demonstrated by the synthesis of $BaSe_3$ from a $BaCl_2$ precursor using the sulfur-$HfH_2$-$K_2S$ system (see **Figure 3.d**). The X-ray diffraction pattern of $BaSe_3$ shows a clear orientation and has been indexed in Supporting Information **Figure S9**. Additionally, Energy Dispersive X-ray (EDX) analysis indicates a Ba to Se ratio of nearly 1:3, confirming the formation of $BaSe_3$ (see **Figure S10**). We also recorded the Raman spectrum of the sample; however, due to the lack of any reported Raman data for $BaSe_3$ in the literature, we were unable to verify it (see **Figure S11**). It is important to note that while we have used $HfH_2$ as a precursor for generating in-situ $H_2S$, other metal hydrides can also be employed. However, $HfH_2$ is particularly essential when synthesizing metal chalcogenides involving highly oxophilic metals.

### *3.3. Synthesis of $BaMS_3$ (M=Ti, Zr, and Hf) compounds from chloride precursors*

The synthesis of $BaMS_3$ compounds from cost-effective precursors will accelerate research on these materials for various optoelectronic applications. With this goal in mind, we expanded the synthesis of BaS film from $BaCl_2$ to the novel synthesis of $BaMS_3$ thin films using a mixed chloride precursor molecular ink. $BaCl_2$ and $ZrCl_4$ were co-dissolved in thiourea-DMF to form soluble complexes. Previous work from our group has demonstrated that thiourea interacts with $ZrCl_4$ to form an adduct in the solution.[49] While a similar interaction is anticipated for $BaCl_2$ dissolution, it could not be confirmed via liquid Raman spectroscopy due to significant fluorescence from the $BaCl_2$ solution. Nevertheless, this marks the first report of the co-dissolution of barium and zirconium chloride precursors in a benign thiourea-DMF solution system. The resulting solution was blade-coated onto a glass substrate and annealed on a hotplate set at 350°C. These coating and annealing steps were repeated 12 times to achieve the desired film thickness. The sulfurization attempt of this film without $K_2S$ and only $HfH_2$ and sulfur resulted in $BaCl_2$ and $ZrS_3$ after sulfurization (illustrated in **Figure 4.a**). The XRF measurements confirmed the presence of Ba, Zr, S, and Cl in the sample (see **Figure S12**). However, the annealed film, containing Ba and Zr precursors, was then sulfurized in an ampule at 575°C for 36 hours with sulfur in the presence of $HfH_2$ and $K_2S$. X-ray diffraction analysis confirm the achievement of phase-pure $BaZrS_3$ with no impurities of $BaCl_2$, a milestone never before attained using chloride precursors (see **Figure 4.a**).

Raman spectroscopy is a valuable complementary technique for detecting materials with small crystalline domains that are not observable via X-ray diffraction or those with overlapping diffraction peaks. The Raman peak positions for $BaZrS_3$, as shown in **Figure 4b** and summarized in **Table 2**, are consistent with literature values. Notably, Pandey et al. identified a peak around 637 $cm^{-1}$, attributing it to the incomplete conversion of $BaZrO_3$ to $BaZrS_3$ in their synthesis.[50] However, as our method does not involve a $BaZrO_3$ intermediate and no other $BaZrO_3$-related peaks were detected, further investigation into the origin of this peak is required. Additionally, many solution-based methods for synthesizing chalcogenide semiconductors often encounter carbon impurities, which can be identified in Raman spectra by peaks around 1300 and 1600 $cm^{-1}$. The minimal residual carbon in our method is also a significant achievement over the previously reported solution-deposited methods for $BaZrS_3$. EDX results further confirm uniform Ba, Zr, and S within the grains and the absence of residual chlorine in the film (see **Figure 4.c-f and S13**). It should be noted that a sulfurization time as short as 3 hours was sufficient to produce phase-pure $BaZrS_3$ (shown in **Figure**

**S14**). However, longer sulfurization durations were chosen to maintain consistency across all the materials synthesized in this study.

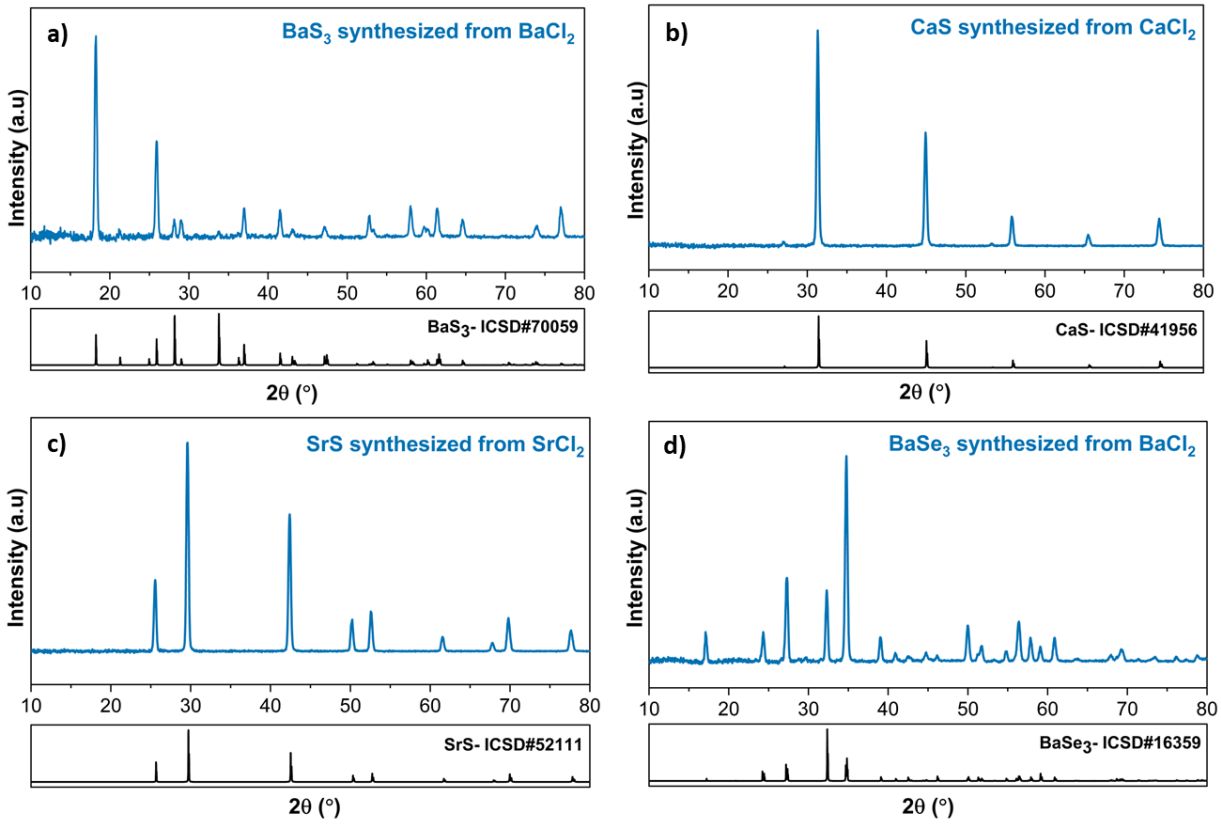


**Figure 3:** a) $BaS_3$, b) CaS, c) SrS, and d) $BaSe_3$ synthesized from metal chloride-thiourea-DMF ink. The as-coated film was sulfurized at 500°C for 36 hours with $HfH_2$, $K_2S$, and sulfur to remove chlorine impurities from the film.

**Table 2:** Raman modes of synthesized $BaZrS_3$ from metal chloride and metal iodide precursors.

| **Observed Raman Peak Location ($cm^{-1}$) in $BaZrS_3$ synthesized from** | | **Peak Assignment from Pandey et al.**[50] |
|---|---|---|
| **Metal chloride precursors** | **Metal iodide precursors** | |
| 75 | 74 | $A_g^2 + B_{3g}^1$ |
| 90 | 89 | $B_{2g}^3 + A_g^3$ |
| 135 | 134 | $A_g^4$ |
| 190 | 189 | $B_{1g}^3 + B_{2g}^5 + B_{3g}^3$ |
| 215 | 215 | $A_g^6$ |
| 222 | 222 | $B_{2g}^6$ |
| 379 | 381 | $2_{\mathrm{ph}}$ |
| 423 | 422 | $B_{1g}^5$ |
| 458 | 453 | $B_{2g}^7 + B_{3g}^5$ |
| 618 | 621 | $X_1$ |

| | | |
|---|---|---|
| 637 | 637 | $BaZrO_3 - E_g$ |
| 819 | 818 | $X_2$ |

However, SEM analysis reveals the formation of islands of $BaZrS_3$ rather than a continuous film, highlighting a challenge common to all $BaMS_3$ synthesis routes (depicted in **Figure S15**). This challenge primarily arises from the difficulty in directly nucleating $BaZrS_3$ during annealing on a hotplate, which necessitates heat treatment in a sulfur-rich environment to generate a $BaS_x$ ($x > 3$) liquid flux for $BaZrS_3$ grain nucleation and growth. Unfortunately, no method has been reported to date for controlling the excess liquid flux, leading to uncontrolled grain growth during sulfurization. Our current approach faces a similar issue, likely due to excess $BaS_x$ flux generated during sulfurization. Therefore, further efforts are required to limit the liquid flux or to use an alternative transport agent to control grain growth. The bandgap of $BaZrS_3$ is generally reported to be between 1.7 and 1.9 eV, with an accepted value around 1.8 eV.[25,49,51,52] The Kubelka-Munk transformation of the diffuse reflectance spectra in **Figure 4g** indicates a bandgap of 1.83 eV for $BaZrS_3$ synthesized from metal chloride precursors, which aligns with this expected range.

The success achieved in synthesizing $BaZrS_3$ films from chloride precursors was readily extended to $BaTiS_3$ and chalcogenide perovskites $BaHfS_3$, as evidenced in **Figures 4.h S16, 5.a and S17**. The Kubelka-Munk transformation on the diffuse reflectance spectrum of $BaHfS_3$ in **Figure 5.b** suggests a bandgap of 2.1 eV, which also makes $BaHfS_3$ interesting for optoelectronic applications. This estimation of the bandgap aligns with the values reported in the literature.[25] Overall, using the $K_2S$-$H_2S$ shuttle has proven to be a remarkable method for synthesizing $BaMS_3$ compounds from cost-effective precursors, eliminating any chlorine and carbon impurities. Moreover, it should be noted that this method produced $BaMS_3$ films at temperatures consistent with those reported in the chalcogenide perovskite literature, where only direct nanoparticle synthesis has been demonstrated at temperatures between 300 and 360 °C, while bulk material synthesis typically requires temperatures above 550 °C, and in most cases, above 800 °C.[36,40,49,53,54]

### *3.4. Synthesis of $BaZrS_3$ from iodide precursors*

In addition to chlorides, iodides are also commonly utilized as cost-effective precursors. Similar to chlorides, no solution-processed synthesis using iodide precursors has been demonstrated for $BaZrS_3$. Like chlorides, alkaline earth metals exhibit a high affinity for iodides, making direct sulfurization of $BaI_2$ precursors ineffective. However, our thermodynamic calculations indicate that potassium has a higher affinity for iodine than barium, suggesting the feasibility of iodine shuttle from barium to potassium using a shuttle gas (see **Table S7**). Consequently, we employed the $K_2S$-$H_2S$ system, similar to the chloride precursor film, to facilitate the iodine shuttle from the as-annealed film to potassium during the sulfurization step. The as-coated film from the $BaI_2$ precursor has residual iodine, as confirmed by the XRF measurement (see **Figure S18**). The successful implementation of the sulfurization method with $HfH_2$, $K_2S$, and sulfur resulted in the synthesis of phase-pure $BaS_3$ and SrS from iodide precursors (depicted in **Figures S19 and S20**). The $BaS_3$ obtained using this method is highly oriented.

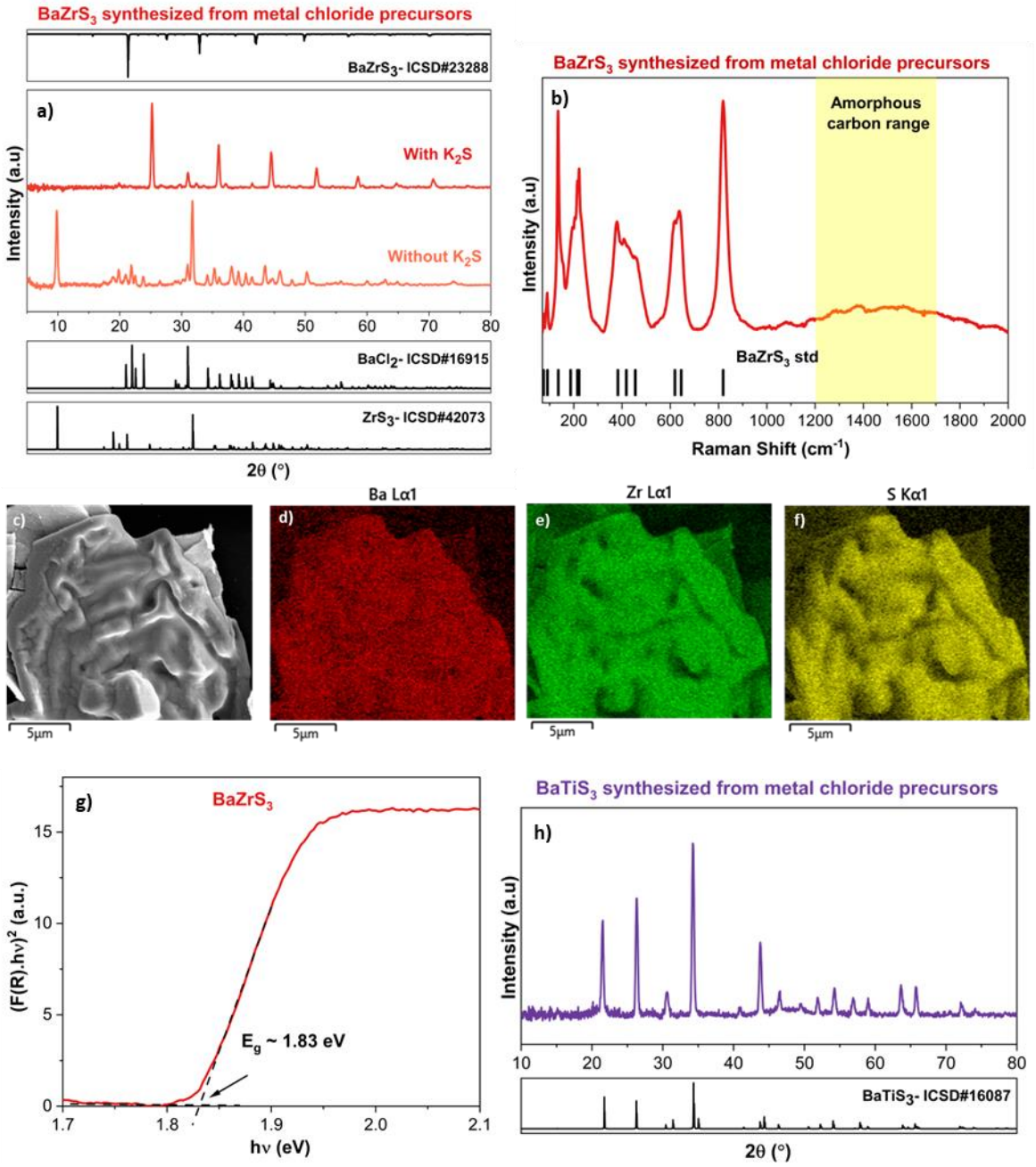


**Figure 4:** The synthesis of $BaZrS_3$ and $BaTiS_3$ using chloride precursors. a) X-ray diffraction patterns with and without the presence of $K_2S$, b) Raman spectrum, c-f) SEM image and EDX maps, g) Kubelka-Munk transformation on the diffuse reflectance spectrum of $BaZrS_3$ synthesized from metal chloride precursors in the presence of $K_2S$ chlorine sink, h) X-ray diffraction of $BaTiS_3$ synthesized from metal chloride precursors. The films were sulfurized at 575°C for 36 hours in the presence of $HfH_2$, $K_2S$, and sulfur.

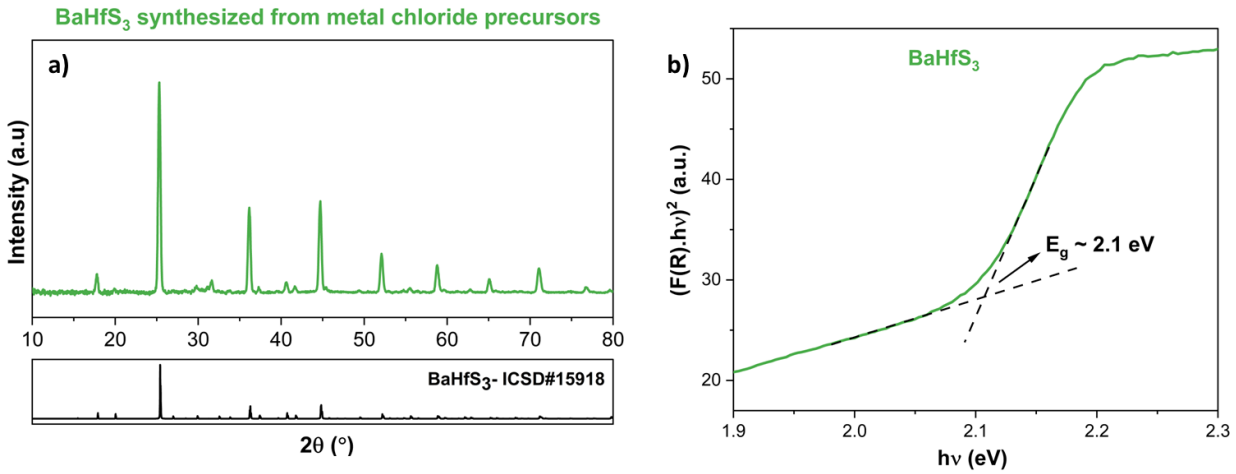


**Figure 5:** $BaHfS_3$ synthesized from metal chloride precursors in the presence of $K_2S$ chlorine sink. a) X-ray diffraction pattern, b) Kubelka-Munk transformation on the diffuse reflectance spectrum. The film was sulfurized at 575°C for 36 hours in the presence of $HfH_2$, $K_2S$, and sulfur.

We further demonstrated a successful implementation of this method to form $BaZrS_3$ from iodide precursors. Initially, a mixed precursor ink containing $BaI_2$ and $ZrI_4$ was formulated in DMF, with thiourea serving as the sulfur source. Analogous to chlorides, thiourea is expected to interact with the iodide precursors in the solution, thereby establishing metal-sulfur bonds. Subsequently, the prepared solution underwent blade coating and annealing on a hotplate set at 350ºC, with this coating-annealing cycle repeated 12 times to achieve the desired film thickness. The resulting as-annealed film underwent sulfurization with sulfur in the presence of $HfH_2$ and $K_2S$, facilitating the transfer of iodine to potassium and yielding phase-pure $BaZrS_3$, as confirmed by X-ray diffraction and Raman spectrum in **Figures 6.a and 6.b**. **Table 2** presents the assignment of various Raman peaks. SEM-EDX maps confirmed the absence of residual chlorine in the film and uniform distribution of Ba, Zr, and S in the grains, albeit with a cracked film, as illustrated in **Figure 6.c-f, S21, and S22**. Furthermore, Raman analysis revealed minimal residual carbon in the film, which is important for utilizing this route for optoelectronics.

### *3.5. Synthesis of $Cu_2BaSnS_4$ from chloride precursors*

The abundance of earth's constituent elements is a crucial factor influencing any semiconductor material's widespread adoption and scalability. $Cu_2BaSnS_4$ excels in this criterion as it comprises elements abundant in the earth's crust and has been demonstrated to be more defect-resistant compared to $Cu_2ZnSnSe_4$, rendering it an intriguing material for photovoltaic applications.[55,56] However, traditionally, this material has been synthesized using costly vacuum-processing techniques.[57,58] Here, we extend our $K_2S$-$H_2S$ shuttle method to synthesize a solution-processed film of $Cu_2BaSnS_4$ from cost-effective metal chloride precursors. A mixed precursor ink containing CuCl, $BaCl_2$, and $SnCl_2$ was prepared in DMF, with thiourea serving as the sulfur source and a mechanism to dissolve the metal chloride precursors in DMF. Subsequently, the ink was coated onto a glass substrate and sulfurized with sulfur in the presence of $HfH_2$ and $K_2S$ at 575ºC for 36 hours, resulting in the phase-pure synthesis of $Cu_2BaSnS_4$, as confirmed by X-ray diffraction (see **Figure 7.a**). The estimated bandgap using the Kubelka Munk transformation on diffuse reflectance data also matches with the reported bandgap for $Cu_2BaSnS_4$ in the literature.[59–62] This achievement is significant, as $Cu_2BaSnS_4$, along with chalcogenide perovskites, represents emerging chalcogenide semiconductors

currently under exploration for various applications. This report thus addresses a barrier in synthesizing these promising compounds from cost-effective metal chloride precursors. It should be noted that while $Cu_2BaSnS_4$ has been successfully nucleated on a hot plate at temperatures below 400 °C and nanoparticles have been synthesized at temperatures below 100 °C, we only attempted synthesis at 575 °C to maintain consistency with the temperature used in this study for synthesizing other compounds. It is likely that $Cu_2BaSnS_4$ can be synthesized at much lower temperatures using the method discussed here.[63–65]

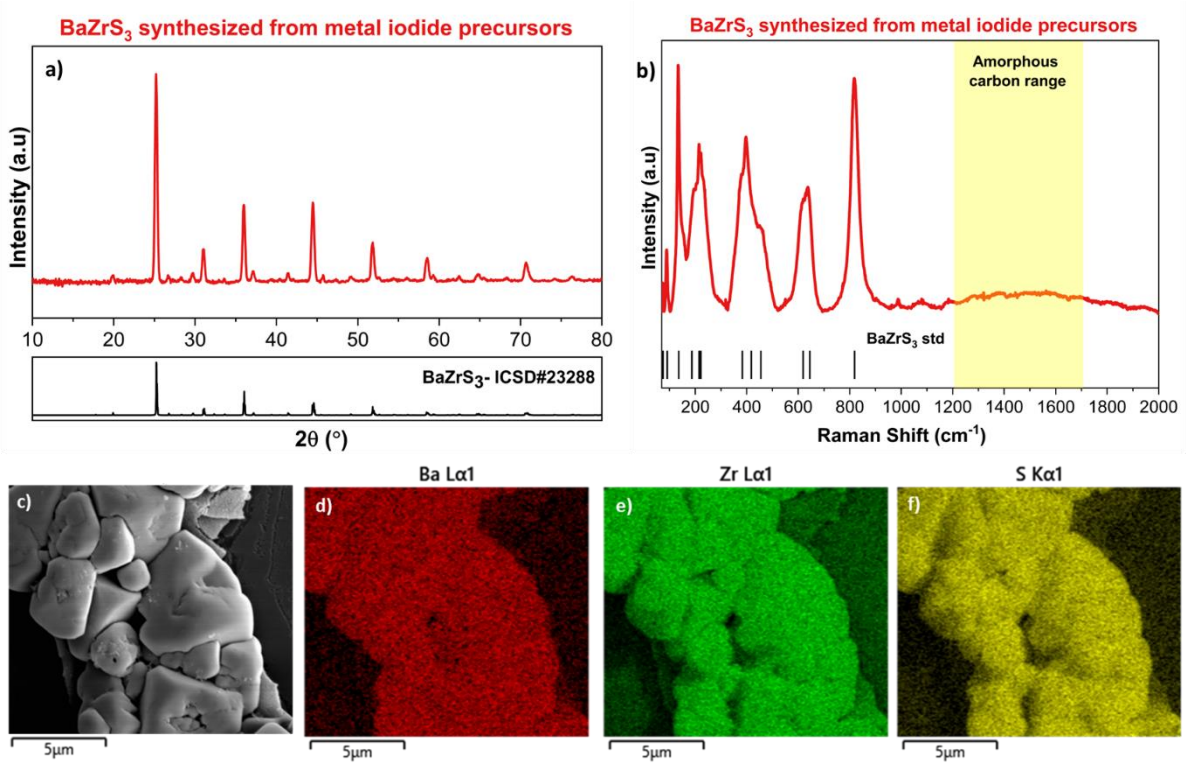


**Figure 6:** $BaZrS_3$ film from iodide precursors. a) X-ray diffraction pattern, b) Raman spectrum, c-f) SEM image and EDX maps. The film was sulfurized at 575°C for 36 hours in the presence of $HfH_2$, $K_2S$, and sulfur.

### *3.6. Other chalcogenides synthesis*

The remarkable $K_2S$-$H_2S$ shuttle can also be utilized to synthesize various other emerging chalcogenides containing alkaline earth metals and sodium from metal halide precursors. Examples include $Ba_2ZnS_3$, $Ba_2MnS_3$, $BaMg_2S_4$, $BaCdSnS_4$, $NaBiS_2$, and other strontium- and calcium-based chalcogenide perovskites. The supporting information (SI) contains discussions on the synthesis of $BaIn_2S_4$ (see **Figure S23**).

## 4. Conclusions

This study conducted thermodynamic calculations to assess the affinity of various elements in the periodic table for chlorine and iodine versus sulfur, yielding scales for the chloriphilicity and iodiphilicity of these elements. The scales revealed that alkali metals exhibit a higher affinity for chlorine and iodine compared to alkaline earth metals. Leveraging these scales, the study introduced a novel $K_2S$-$H_2S$ system, supported by temperature-dependent thermodynamic calculations, to facilitate the transfer of chlorine and iodine from

alkaline earth metals to potassium during sulfurization. This innovative approach led to the synthesis of phase-pure alkaline earth metal-containing chalcogenide materials from chloride and iodide metal precursors. Furthermore, the methodology was extended to encompass a variety of chalcogenide materials, including both sulfides and selenides.

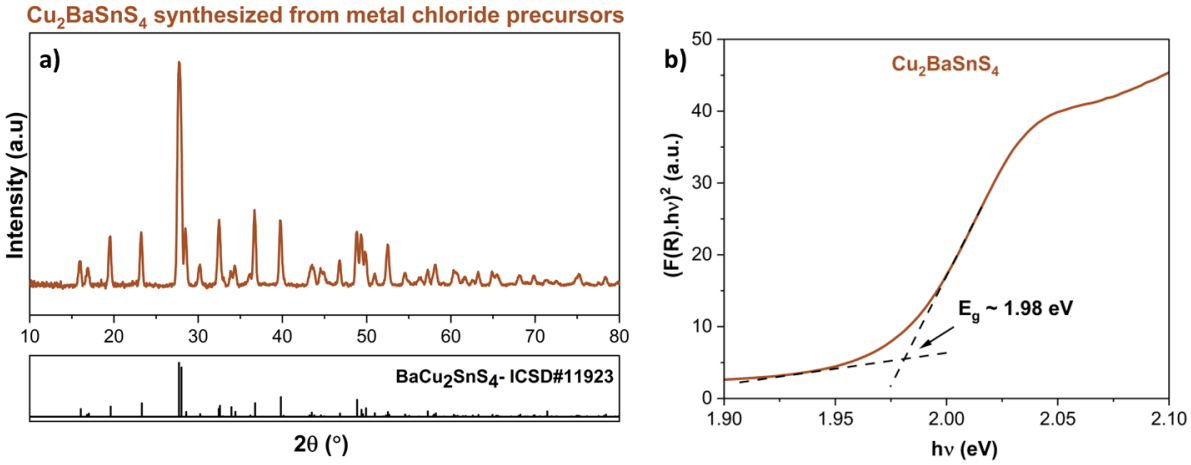


**Figure 7:** $Cu_2BaSn_4$ synthesized from metal chloride precursors. a) X-ray diffraction pattern, b) Kubelka-Munk transformation on the diffuse reflectance spectrum. The film was sulfurized at 575°C for 36 hours in the presence of $HfH_2$, $K_2S$, and sulfur.

## CRediT authorship contribution statement

**S. Agarwal:** Writing – original draft, Writing – review & editing, Validation, Methodology, Investigation, Formal analysis, Data curation, Visualization, Conceptualization. **K.C. Vincent:** Writing – review & editing, Validation, Methodology, Investigation, Formal analysis, Data curation. **R. Agrawal:** Writing – review & editing, Validation, Supervision, Resources, Methodology, Funding acquisition.

## Conflict of Interest

The authors declare no conflict of interest.

## Data Availability

The data supporting this article have been included in the Supporting Information.

## Supporting Information

Information on additional X-ray diffraction, Raman, EDX, and UV-vis data are provided in the supporting information.

## Acknowledgments

The authors acknowledge the National Science Foundation's financial support through Grant 10001536 (INFEWS). Special thanks are extended to Dr. Jonathan Turnley for his valuable discussions regarding the project.

**References**

(1) Wada, T.; Nakamura, S.; Maeda, T. Ternary and Multinary Cu-chalcogenide Photovoltaic Materials from CuInSe2 to Cu2ZnSnS4 and Other Compounds. *Prog Photovolt Res Appl* 2012, *20* (5), 520–525. https://doi.org/10.1002/pip.2183.

(2) van der Stam, W.; Berends, A. C.; de Mello Donega, C. Prospects of Colloidal Copper Chalcogenide Nanocrystals. *ChemPhysChem* 2016, *17* (5), 559–581. https://doi.org/10.1002/cphc.201500976.

(3) Kim, S.; Lee, Y.-I.; Choi, Y.-M.; Lim, H.-R.; Lim, J.-H.; Myung, N. V; Choa, Y.-H. Thermochemical Hydrogen Sensor Based on Chalcogenide Nanowire Arrays. *Nanotechnology* 2015, *26* (14), 145503. https://doi.org/10.1088/0957-4484/26/14/145503.

(4) Sharma, I.; Pawar, P. S.; Kumar Yadav, R.; Nandi, R.; Heo, J. Review on Bandgap Engineering in Metal-Chalcogenide Absorber Layer via Grading: A Trend in Thin-Film Solar Cells. *Solar Energy* 2022, *246*, 152–180. https://doi.org/10.1016/j.solener.2022.09.046.

(5) Paire, M.; Delbos, S.; Vidal, J.; Naghavi, N.; Guillemoles, J. F. Chalcogenide Thin-Film Solar Cells. In *Solar Cell Materials*; Wiley, 2014; pp 145–215. https://doi.org/10.1002/9781118695784.ch7.

(6) Daume, F.; Puttnins, S.; Scheit, C.; Zachmann, H.; Rahm, A.; Braun, A.; Grundmann, M. Damp Heat Treatment of Cu(In,Ga)Se2 Solar Cells with Different Sodium Content. *Materials* 2013, *6* (12), 5478–5489. https://doi.org/10.3390/ma6125478.

(7) McLeod, S. M.; Hages, C. J.; Carter, N. J.; Agrawal, R. Synthesis and Characterization of 15% Efficient CIGSSe Solar Cells from Nanoparticle Inks. *Prog Photovolt Res Appl* 2015, *23* (11), 1550–1556. https://doi.org/10.1002/pip.2588.

(8) Hages, C. J.; Carter, N. J.; Agrawal, R. Generalized Quantum Efficiency Analysis for Non-Ideal Solar Cells: Case of Cu2ZnSnSe4. *J Appl Phys* 2016, *119* (1), 014505. https://doi.org/10.1063/1.4939487.

(9) Mavlonov, A.; Razykov, T.; Raziq, F.; Gan, J.; Chantana, J.; Kawano, Y.; Nishimura, T.; Wei, H.; Zakutayev, A.; Minemoto, T.; Zu, X.; Li, S.; Qiao, L. A Review of Sb2Se3 Photovoltaic Absorber Materials and Thin-Film Solar Cells. *Solar Energy* 2020, *201*, 227–246. https://doi.org/10.1016/j.solener.2020.03.009.

(10) Ellis, R. G.; Turnley, J. W.; Rokke, D. J.; Fields, J. P.; Alruqobah, E. H.; Deshmukh, S. D.; Kisslinger, K.; Agrawal, R. Hybrid Ligand Exchange of Cu(In,Ga)S2 Nanoparticles for

Carbon Impurity Removal in Solution-Processed Photovoltaics. *Chem Mat* 2020, *32* (12), 5091–5103. https://doi.org/10.1021/acs.chemmater.0c00966.

(11) Hages, C. J.; Agrawal, R. Synthesis of CZTSSe Thin Films from Nanocrystal Inks. In *Copper Zinc Tin Sulfide-Based Thin-Film Solar Cells*; John Wiley & Sons Ltd: Chichester, UK, 2015; pp 239–270. https://doi.org/10.1002/9781118437865.ch11.

(12) Deshmukh, S. D.; Weideman, K. G.; Ellis, R. G.; Kisslinger, K.; Agrawal, R. Enabling Fine-Grain Free 2-Micron Thick CISe/CIGSe Film Fabrication *via* a Non-Hydrazine Based Solution Processing Route. *Mater Adv* 2022, *3* (7), 3293–3302. https://doi.org/10.1039/D2MA00095D.

(13) Lepetit, T.; Harel, S.; Arzel, L.; Ouvrard, G.; Barreau, N. KF Post Deposition Treatment in Co-Evaporated Cu(In,Ga)Se2 Thin Film Solar Cells: Beneficial or Detrimental Effect Induced by the Absorber Characteristics. *Prog Photovolt Res Appl* 2017, *25* (12), 1068–1076. https://doi.org/10.1002/pip.2924.

(14) Wang, W.; Mark, W. T.; Gunawan, O.; Gokmen, T.; Todorov, T. K.; Zhu, Y.; Mitzi, D. B. Device Characteristics of CZTSSe Thin-Film Solar Cells 12.6% Efficiency. *Adv Energy Mater* 2014, *4*. https://doi.org/10.1002/aenm.201301465.

(15) Zhang, T.; Yang, Y.; Liu, D.; Tse, S. C.; Cao, W.; Feng, Z.; Chen, S.; Qian, L. High Efficiency Solution-Processed Thin-Film Cu(In,Ga)(Se,S)2 Solar Cells. *Energy Environ Sci* 2016, *9* (12), 3674–3681. https://doi.org/10.1039/C6EE02352E.

(16) Suresh, S.; Uhl, A. R. Present Status of Solution-Processing Routes for Cu(In,Ga)(S,Se)2 Solar Cell Absorbers. *Adv Energy Mater* 2021, *11* (14), 2003743. https://doi.org/10.1002/aenm.202003743.

(17) Turnley, J. W.; Agrawal, R. Solution Processed Metal Chalcogenide Semiconductors for Inorganic Thin Film Photovoltaics. *Chem Commun* 2024, *60* (40), 5245–5269. https://doi.org/10.1039/D4CC01057D.

(18) Agarwal, S.; Weideman, K.; Rokke, D.; Vincent, K. C.; Zemlyanov, D.; Agrawal, R. Enhancing the Optoelectronic Properties of Solution-Processed AgInSe2 Thin Films for Application in Photovoltaics. *J Mater Chem C Mater* 2024, *12* (1), 325–336. https://doi.org/10.1039/D3TC03540A.

(19) Mitzi, D. B.; Yuan, M.; Liu, W.; Kellock, A. J.; Chey, S. J.; Gignac, L.; Schrott, A. G. Hydrazine-Based Deposition Route for Device-Quality CIGS Films. *Thin Solid Films* 2009, *517* (7), 2158–2162. https://doi.org/10.1016/j.tsf.2008.10.079.

(20) Zhao, X.; Deshmukh, S. D.; Rokke, D. J.; Zhang, G.; Wu, Z.; Miller, J. T.; Agrawal, R. Investigating Chemistry of Metal Dissolution in Amine−Thiol Mixtures and Exploiting It

toward Benign Ink Formulation for Metal Chalcogenide Thin Films. *Chem Mater* 2019, *31* (15), 5674–5682. https://doi.org/10.1021/acs.chemmater.9b01566.

(21) Clark, J. A.; Murray, A.; Lee, J.; Autrey, T. S.; Collord, A. D.; Hillhouse, H. W. Complexation Chemistry in N,N -Dimethylformamide-Based Molecular Inks for Chalcogenide Semiconductors and Photovoltaic Devices. *J Am Chem Soc* 2019, *141* (1), 298–308. https://doi.org/10.1021/jacs.8b09966.

(22) Niu, C.; Gong, Y.; Qiu, R.; Zhu, Q.; Zhou, Y.; Hao, S.; Yan, W.; Huang, W.; Xin, H. 11.5% Efficient Cu2ZnSn(S,Se)4 Solar Cell Fabricated from DMF Molecular Solution. *J Mater Chem A Mater* 2021, *9* (22), 12981–12987. https://doi.org/10.1039/D1TA01871J.

(23) Raj, R.; Singh, R.; Guin, M. Chalcogenide Perovskite, An Emerging Photovoltaic Material: Current Status and Future Perspectives. *ChemistrySelect* 2023, *8* (45). https://doi.org/10.1002/slct.202303550.

(24) Hanzawa, K.; Iimura, S.; Hiramatsu, H.; Hosono, H. Material Design of Green-Light-Emitting Semiconductors: Perovskite-Type Sulfide SrHfS3. *J Am Chem Soc* 2019, *141* (13), 5343–5349. https://doi.org/10.1021/jacs.8b13622.

(25) Sopiha, K. V; Comparotto, C.; Márquez, J. A.; Scragg, J. J. S. Chalcogenide Perovskites: Tantalizing Prospects, Challenging Materials. *Adv Optical Mater* December 13, 2022, p 2101704. https://doi.org/10.1002/adom.202101704.

(26) Teymur, B.; Levcenco, S.; Hempel, H.; Bergmann, E.; Márquez, J. A.; Choubrac, L.; Hill, I. G.; Unold, T.; Mitzi, D. B. Optoelectronic and Material Properties of Solution-Processed Earth-Abundant Cu2BaSn(S, Se)4 Films for Solar Cell Applications. *Nano Energy* 2021, *80*, 105556. https://doi.org/10.1016/j.nanoen.2020.105556.

(27) Shin, D.; Zhu, T.; Huang, X.; Gunawan, O.; Blum, V.; Mitzi, D. B. Earth-Abundant Chalcogenide Photovoltaic Devices with over 5% Efficiency Based on a Cu2BaSn(S,Se)4 Absorber. *Adv Mater* 2017, *29* (24). https://doi.org/10.1002/adma.201606945.

(28) Eya, H. I.; Dzade, N. Y. Density Functional Theory Insights into the Structural, Electronic, Optical, Surface, and Band Alignment Properties of BaZrS3 Chalcogenide Perovskite for Photovoltaics. *ACS Appl Energy Mater* 2023, *6* (11), 5729–5738. https://doi.org/10.1021/acsaem.3c00103.

(29) Ju, M.; Dai, J.; Ma, L.; Zeng, X. C. Perovskite Chalcogenides with Optimal Bandgap and Desired Optical Absorption for Photovoltaic Devices. *Adv Energy Mater* 2017, *7* (18), 1700216. https://doi.org/10.1002/aenm.201700216.

(30) Nishigaki, Y.; Nagai, T.; Nishiwaki, M.; Aizawa, T.; Kozawa, M.; Hanzawa, K.; Kato, Y.; Sai, H.; Hiramatsu, H.; Hosono, H.; Fujiwara, H. Extraordinary Strong Band-Edge Absorption

in Distorted Chalcogenide Perovskites. *Solar RRL* 2020, *4* (5), 1900555. https://doi.org/10.1002/solr.201900555.

(31) Zhu, T.; Huhn, W. P.; Wessler, G. C.; Shin, D.; Saparov, B.; Mitzi, D. B.; Blum, V. I 2 –II–IV–VI 4 (I = Cu, Ag; II = Sr, Ba; IV = Ge, Sn; VI = S, Se): Chalcogenides for Thin-Film Photovoltaics. *Chem Mater* 2017, *29* (18), 7868–7879. https://doi.org/10.1021/acs.chemmater.7b02638.

(32) Niu, S.; Zhao, B.; Ye, K.; Bianco, E.; Zhou, J.; McConney, M. E.; Settens, C.; Haiges, R.; Jaramillo, R.; Ravichandran, J. Crystal Growth and Structural Analysis of Perovskite Chalcogenide BaZrS3 and Ruddlesden–Popper Phase Ba3Zr2S7. *J Mater Res* 2019, *34* (22), 3819–3826. https://doi.org/10.1557/jmr.2019.348.

(33) Surendran, M.; Chen, H.; Zhao, B.; Thind, A. S.; Singh, S.; Orvis, T.; Zhao, H.; Han, J.-K.; Htoon, H.; Kawasaki, M.; Mishra, R.; Ravichandran, J. Epitaxial Thin Films of a Chalcogenide Perovskite. *Chem Mater* 2021, *33* (18), 7457–7464. https://doi.org/10.1021/acs.chemmater.1c02202.

(34) Comparotto, C.; Davydova, A.; Ericson, T.; Riekehr, L.; Moro, M. V.; Kubart, T.; Scragg, J. Chalcogenide Perovskite BaZrS3: Thin Film Growth by Sputtering and Rapid Thermal Processing. *ACS Appl Energy Mater* 2020, *3* (3), 2762–2770. https://doi.org/10.1021/acsaem.9b02428.

(35) Vincent, K. C.; Agarwal, S.; Turnley, J. W.; Agrawal, R. Liquid Flux–Assisted Mechanism for Modest Temperature Synthesis of Large-Grain BaZrS3 and BaHfS3 Chalcogenide Perovskites. *Adv Energy Sustainability Res* 2023, *4* (5). https://doi.org/10.1002/aesr.202300010.

(36) Yang, R.; Nelson, J.; Fai, C.; Yetkin, H. A.; Werner, C.; Tervil, M.; Jess, A. D.; Dale, P. J.; Hages, C. J. A Low-Temperature Growth Mechanism for Chalcogenide Perovskites. *Chem Mater* 2023, *35* (12), 4743–4750. https://doi.org/10.1021/acs.chemmater.3c00494.

(37) Turnley, J. W.; Vincent, K. C.; Pradhan, A. A.; Panicker, I.; Swope, R.; Uible, M. C.; Bart, S. C.; Agrawal, R. Solution Deposition for Chalcogenide Perovskites: A Low-Temperature Route to BaMS3 Materials (M = Ti, Zr, Hf). *J Am Chem Soc* 2022, *144* (40), 18234–18239. https://doi.org/10.1021/jacs.2c06985.

(38) Pradhan, A. A.; Uible, M. C.; Agarwal, S.; Turnley, J. W.; Khandelwal, S.; Peterson, J. M.; Blach, D. D.; Swope, R. N.; Huang, L.; Bart, S. C.; Agrawal, R. Synthesis of BaZrS3 and BaHfS3 Chalcogenide Perovskite Films Using Single-Phase Molecular Precursors at Moderate Temperatures. *Angew Chem Int Ed* 2023, 62 (15), e202301049. https://doi.org/10.1002/anie.202301049.

(39) Zilevu, D.; Creutz, S. E. Shape-Controlled Synthesis of Colloidal Nanorods and Nanoparticles of Barium Titanium Sulfide. *Chem Mater* 2021, *33* (13), 5137–5146. https://doi.org/10.1021/acs.chemmater.1c01193.

(40) Zilevu, D.; Parks, O. O.; Creutz, S. E. Solution-Phase Synthesis of the Chalcogenide Perovskite Barium Zirconium Sulfide as Colloidal Nanomaterials. *Chem Commun* 2022, *58* (75), 10512–10515. https://doi.org/10.1039/D2CC03494H.

(41) Ravi, V. K.; Yu, S. H.; Rajput, P. K.; Nayak, C.; Bhattacharyya, D.; Chung, D. S.; Nag, A. Colloidal BaZrS3 Chalcogenide Perovskite Nanocrystals for Thin Film Device Fabrication. *Nanoscale* 2021, *13* (3), 1616–1623. https://doi.org/10.1039/D0NR08078K.

(42) Teymur, B.; Zhou, Y.; Ngaboyamahina, E.; Glass, J. T.; Mitzi, D. B. Solution-Processed Earth-Abundant Cu2BaSn(S,Se)4 Solar Absorber Using a Low-Toxicity Solvent. *Chem Mater* 2018, *30* (17), 6116–6123. https://doi.org/10.1021/acs.chemmater.8b02556.

(43) Larentzos, J. P.; Criscenti, L. J. A Molecular Dynamics Study of Alkaline Earth Metal−Chloride Complexation in Aqueous Solution. *J Phys Chem B* 2008, *112* (45), 14243–14250. https://doi.org/10.1021/jp802771w.

(44) Hildenbrand, D. L. Dissociation Energies and Chemical Bonding in the Alkaline-Earth Chlorides from Mass Spectrometric Studies. *J Chem Phys* 1970, *52* (11), 5751–5759. https://doi.org/10.1063/1.1672855.

(45) Mills, K. C. *Thermodynamic Data for Inorganic Sulphides, Selenides and Tellurides*; The Butterworth Group: London, 1974.

(46) Rumble Jr., J. R.; Lide, D. R.; Bruno, T. J. *CRC Handbook of Chemistry and Physics*, 98th edition.; CRC Press, 2017.

(47) NIST Chemistry WebBook, SRD 69. 2023. https://doi.org/10.18434/T4D303

(48) Agarwal, S.; Turnley, J. W.; Pradhan, A. A.; Agrawal, R. Moderate Temperature Sulfurization and Selenization of Highly Stable Metal Oxides: An Opportunity for Chalcogenide Perovskites. *J Mater Chem C Mater* 2023, *11* (45), 15817–15823. https://doi.org/10.1039/D3TC02716C.

(49) Vincent, K. C.; Agarwal, S.; Fan, Z.; Canizales, A. S. M.; Agrawal, R. Expanding the Horizons for Viable Precursors and Liquid Fluxes for the Synthesis of BaZrS3 and Related Compounds. *J Mater Chem C Mater* 2024, *12*, 12521-12534. https://doi.org/10.1039/D4TC02287D

(50) Pandey, J.; Ghoshal, D.; Dey, D.; Gupta, T.; Taraphder, A.; Koratkar, N.; Soni, A. Local Ferroelectric Polarization in Antiferroelectric Chalcogenide Perovskite BaZrS3 Thin Films. *Phys Rev B* 2020, *102* (20), 205308. https://doi.org/10.1103/PhysRevB.102.205308.

(51) Gupta, T.; Ghoshal, D.; Yoshimura, A.; Basu, S.; Chow, P. K.; Lakhnot, A. S.; Pandey, J.; Warrender, J. M.; Efstathiadis, H.; Soni, A.; Osei-Agyemang, E.; Balasubramanian, G.; Zhang, S.; Shi, S.; Lu, T.; Meunier, V.; Koratkar, N. An Environmentally Stable and Lead-Free Chalcogenide Perovskite. *Adv Funct Mater* 2020, *30* (23), 2001387. https://doi.org/10.1002/adfm.202001387.

(52) Sadeghi, I.; Ye, K.; Xu, M.; Li, Y.; LeBeau, J. M.; Jaramillo, R. Making BaZrS3 Chalcogenide Perovskite Thin Films by Molecular Beam Epitaxy. *Adv Funct Mater* 2021, *31* (45), 2105563. https://doi.org/10.1002/adfm.202105563.

(53) Yang, R.; Jess, A. D.; Fai, C.; Hages, C. J. Low-Temperature, Solution-Based Synthesis of Luminescent Chalcogenide Perovskite BaZrS3 Nanoparticles. *J Am Chem Soc* 2022, *144* (35), 15928–15931. https://doi.org/10.1021/jacs.2c06168.

(54) Agarwal, S.; Vincent, K. C.; Turnley, J. W.; Hayes, D. C.; Uible, M. C.; Durán, I.; Canizales, A. S. M.; Khandelwal, S.; Panicker, I.; Andoh, Z.; Spilker, R. M.; Ma, Q.; Huang, L.; Hwang, S.; Kisslinger, K.; Svatek, S.; Antolin, E.; Bart, S. C.; Agrawal, R. Breaking Barriers in Chalcogenide Perovskite Synthesis: A Generalized Framework for Fabrication of BaMS3 (M═Ti, Zr, Hf) Materials. *Adv Funct Mater* 2024. Early View. https://doi.org/10.1002/adfm.202405416.

(55) Hong, F.; Lin, W.; Meng, W.; Yan, Y. Trigonal Cu 2 -II-Sn-VI 4 (II = Ba, Sr and VI = S, Se) Quaternary Compounds for Earth-Abundant Photovoltaics. *Phys. Chem. Chem. Phys.* 2016, *18* (6), 4828–4834. https://doi.org/10.1039/C5CP06977G.

(56) Chen, S.; Walsh, A.; Gong, X.; Wei, S. Classification of Lattice Defects in the Kesterite Cu2ZnSnS4 and Cu2ZnSnSe4 Earth-Abundant Solar Cell Absorbers. *Adv Mater* 2013, *25* (11), 1522–1539. https://doi.org/10.1002/adma.201203146.

(57) Sun, J.-P.; Márquez, J. A.; Stange, H.; Mainz, R.; Mitzi, D. B. Phase and Film Formation Pathway for Vacuum-Deposited Cu2BaSn(SSe)4 Absorber Layers. *Phys Rev Mater* 2019, *3* (5), 055402. https://doi.org/10.1103/PhysRevMaterials.3.055402.

(58) Shin, D.; Zhu, T.; Huang, X.; Gunawan, O.; Blum, V.; Mitzi, D. B. Earth-Abundant Chalcogenide Photovoltaic Devices with over 5% Efficiency Based on a Cu2BaSn(S,Se)4 Absorber. *Adv Mater* 2017, *29* (24). https://doi.org/10.1002/adma.201606945.

(59) Ge, J.; Grice, C. R.; Yan, Y. Cu-Based Quaternary Chalcogenide Cu2BaSnS4 Thin Films Acting as Hole Transport Layers in Inverted Perovskite CH3NH3PbI3 Solar Cells. *J Mater Chem A Mater* 2017, *5* (6), 2920–2928. https://doi.org/10.1039/C6TA08426E.

(60) Crovetto, A.; Xing, Z.; Fischer, M.; Nielsen, R.; Savory, C. N.; Rindzevicius, T.; Stenger, N.; Scanlon, D. O.; Chorkendorff, I.; Vesborg, P. C. K. Experimental and First-Principles Spectroscopy of Cu2SrSnS4 and Cu2BaSnS4 Photoabsorbers. *ACS Appl Mater Interfaces* 2020, *12* (45), 50446–50454. https://doi.org/10.1021/acsami.0c14578.

(61) Kim, Y.; Hempel, H.; Levcenco, S.; Euvrard, J.; Bergmann, E.; Gunawan, O.; Unold, T.; Hill, I. G.; Mitzi, D. B. Optoelectronic Property Comparison for Isostructural Cu2BaGeSe4 and Cu2BaSnS4 Solar Absorbers. *J Mater Chem A Mater* 2021, *9* (41), 23619–23630. https://doi.org/10.1039/D1TA05666B.

(62) Luo, H.; Chen, J.; Zhang, X.; Wang, S.; Gu, H.; Wang, W.; Li, H. Controlled Synthesis of High Efficiency Cu2BaSnS4 Solar Cells via a Solution Processed Method. *Mater Lett* 2020, *270*, 127750. https://doi.org/10.1016/j.matlet.2020.127750.

(63) Chakraborty, R.; Sim, K. M.; Shrivastava, M.; Adarsh, K. V.; Chung, D. S.; Nag, A. Colloidal Synthesis, Optical Properties, and Hole Transport Layer Applications of Cu2BaSnS4 (CBTS) Nanocrystals. *ACS Appl Energy Mater* 2019, *2* (5), 3049–3055. https://doi.org/10.1021/acsaem.9b00473.

(64) McCarthy, C. L.; Brutchey, R. L. Solution Deposited Cu2BaSnS4– *x*Se*x* from a Thiol–Amine Solvent Mixture. *Chem Mater* 2018, *30* (2), 304–308. https://doi.org/10.1021/acs.chemmater.7b03931.

(65) Teymur, B.; Kim, Y.; Huang, J.; Sun, K.; Hao, X.; Mitzi, D. B. Top Stack Optimization for Cu2BaSn(S, Se)4 Photovoltaic Cell Leads to Improved Device Power Conversion Efficiency beyond 6%. *Adv Energy Mater* 2022, *12* (40). https://doi.org/10.1002/aenm.202201602.

(66) Makuła, P.; Pacia, M.; Macyk, W. How To Correctly Determine the Band Gap Energy of Modified Semiconductor Photocatalysts Based on UV–Vis Spectra. *J Phys Chem Lett* 2018, *9* (23), 6814–6817. https://doi.org/10.1021/acs.jpclett.8b02892.

(67) Zhong, H.; Pan, F.; Yue, S.; Qin, C.; Hadjiev, V.; Tian, F.; Liu, X.; Lin, F.; Wang, Z.; Bao, J. Idealizing Tauc Plot for Accurate Bandgap Determination of Semiconductor with Ultraviolet–Visible Spectroscopy: A Case Study for Cubic Boron Arsenide. *J Phys Chem Lett* 2023, *14* (29), 6702–6708. https://doi.org/10.1021/acs.jpclett.3c01416.

**For Table of Contents Only**